Control of Vertical Distribution of Thiophene-Based Copolymers Containing 4,7-Dithien-2-yl-benzo[C][1,2,5]thiadiazole and 3,6-Dithien-2-yl-pyrrolo[3,4-C] pyrrole-1,4(2H,5H)-dione as Side Groups for Photovoltaics

Min-Hee Choi, Tae Ho Lee, Yong Woon Han, Doo Kyung Moon

Department of Materials Chemistry and Engineering, Konkuk University, 1 Hwayang-Dong, Gwangjin-Gu, Seoul 143-701, Korea
Correspondence to: D. K. Moon (E-mail: dkmoon@konkuk.ac.kr)

Received 21 March 2016; accepted 27 April 2016; published online 9 June 2016
DOI: 10.1002/pola.28157

ABSTRACT: Four new D—A type copolymers with 2D-conjugated side-chain identified PfToBT, PbToBT, PfTDPP and PbTDPP, containing two acceptors 4,7-dithien-2-yl-benzo[c][1,2,5]thiadiazole (DTBT), and diketopyrrolopyrrole (DPP) linked by thiophene donors, are obtained using Pd-catalyzed Stille-coupling reaction. These polymers show a broad visible-near-infrared absorption band (E_g = 1.79–1.66 eV) and possess a relatively low-lying HOMO level at −5.34 to −5.12 eV. All the polymer:$PC_{70}BM$ blend films showed edge-on structure and have similar d_π-spacing values. According to the structure of conjugated side-chain, the vertical distributions of polymer chains and $PC_{70}BM$ within the BHJ (bulk heterojunction) were different. When DPP used as an acceptor, conjugated side chains of the polymer coexisted with $PC_{70}BM$ in same position. The BHJ film prepared from PfToBT, PbToBT had a discontinuous network between polymer and $PC_{70}BM$, whereas films from PfTDPP and PbTDPP formed continuous and evenly distributed network between them. This optimized vertical morphology promotes hole transport along respective pathways of polymers and fullerenes in the vertical direction, leading to high J_{SC}. PbTDPP shows PCE up to 2.9% (Jsc of 9.4 mA/cm^2, Voc of 0.68 V, and FF of 0.44). © 2016 Wiley Periodicals, Inc. J. Polym. Sci., Part A: Polym. Chem. **2016**, *54*, 2746–2759

KEYWORDS: bulk heterojunctions; conjugated polymers; D-A type polymer; organic solar cells; orientation; phase separation; two-dimensional conjugation; vertical distribution

INTRODUCTION Recently, polymer solar cells(PSCs) have been to the fore at academic and industrial world as promising alternatives to inorganic photovoltaics because of their lightweight, low manufacturing costs, flexibility, and the possibility of large scale production via solution processing.[1] Bulk heterojunction (BHJ) system, which is a blend structure of an electron donor (i.e., conjugated polymer) and an electron-acceptor (i.e., the fullerene), has been widely researched to that end.[2,3] Conditions of a best polymer as the donor in PSCs should be possessed are acknowledged well: low bandgap, high absorption in the visible and near-infrared regions, appropriate molecular orbital levels that line up with the electron-acceptor, high charge mobility, and excellent miscibility with the electron-acceptor that forms a maximizing the interface between the electron-donor and electron-acceptor network. Judiciously coordinating and managing the parameters of the polymer donor can achieve high-efficiency of the PSCs due to high values of short-circuit current density (Jsc), open-circuit voltage (Voc), and fill factor (FF).

The fundamental design of narrow band gap (NBG) polymer is donor–acceptor (D–A) architecture with broad absorption region by identifying the relationship between the structure of the conjugated backbone and photovoltaic property.[4–7] Although the PCE of conventional PSCs is already around 7%, further optimization of various characteristics is necessary to gain better performance.[8] The inverted PSCs have significantly improved long-range air stability, giving rise to PCE values greater than 10% in comparison with conventional PSCs.[9,10] Certainly, both a sensible moleculer design and the optimization of device physics are crucial in the development of high-efficiency PSCs.[11,12]

Two-dimensional (2D)-conjugation and D–A concept have been confirmed a successful theories in development of high-performance electron-donor polymers. 2D-conjugated polymers, such as polythiophenes containing conjugated side chains reported by Li and Tang's group, show low bandgap, higher charge mobility and relatively low-lying HOMO levels, which are suitable properties for high performance conjugated polymer as an electron-donor for PSCs.[13–15] A new series of polymer donors containing conjugated side chains has been successfully achieved in the past few years through

Additional Supporting Information may be found in the online version of this article.

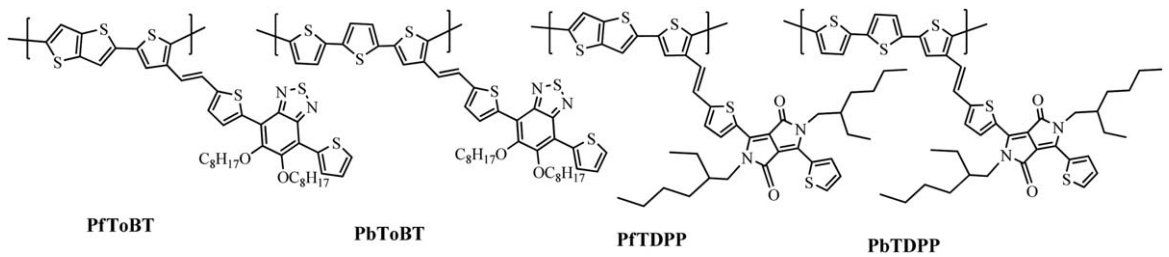

FIGURE 1 Molecular structures of PfToBT, PbToBT, PfTDPP, and PbTDPP.

the efforts of several different research groups. In a previous publication, Tan et al. reported a 2D-conjugated D–A copolymer, PTG1, using 4,7-dithien-2-yl-2,1,3-benzodiathiazole(DTBT) as electron-acceptor and conjugated side chains. PTG1 showed great hole mobility and a best PCE up to ~5%.[16,17] However, its comparatively narrow absorption region and weak absorption coefficient restrict any more enhancement of its photovoltaic performance. Li et al. attached fluorine as a substituent group on the acceptor to expand the absorption region, but the electron withdrawing effect of the fluorinated acceptor unit was very small ($E_g \sim 1.90$ eV). The fluorinated acceptor also limited solubility and molecular weight of the polymer.[13] Majority of these D–A polymers containing conjugated side-chain do not show equivalent photovoltaic properties to their counterpart polymers which have same main-chain components. In order to improve performance of D–A polymers containing conjugated side-chain, it is needed to develop new, stronger conjugated side chains for decreasing the band gap of such polymers.

DTBT and pyrrolo[3,4-c]pyrrole-1,4-dione(DPP) are well-known strong electron-accepting units, and are mostly used to make high-performance D–A copolymers.[18,19] Especially, DPP has several other beneficial attributes including its planar structure, strong electron withdrawing nature and highly conjugated lactam structure (which induces large intermolecular interactions because of π–π stacking between the chains of these polymers), favorable supramolecular order, and increased charge carrier mobility.[20] By varying the donor segments, it has afforded a series of donor–acceptor polymers showing extraordinary hole mobility with the highest value being ~2 [$cm^2/(V\ s)$] and the best photovoltaic device performance being over 5.5%.[21–23] DPP achieves a high degree of coplanarity in the polymer backbone when combined with other aromatic blocks such as thiophene, bithiophene, thienothiophene, naphthalene and benzothidiazole. Such high coplanarity is favorable for efficient charge transport properties and stronger D–A interactions along the conjugated backbone.[24] However, most of theses DPP-based copolymers have low miscibility with fullerene derivatives and need to be processed with additives to achieve desired film morphologies.[25] So DPP-based copolymers need a new conjugation motif that retains their unique advantages.

Among 2D-conjugated D–A polymers, those based on thiophene derivatives containing conjugated acceptor side-chain indicate advantages of enhanced absorption, decreased HOMO energy level and increased hole mobility. Based on the aforementioned points, we designed and synthesized four copolymers of new 2D D–A type copolymers with conjugated side-chain labeled PfToBT, PbToBT, PfTDPP, and PbTDPP (as shown in Fig. 1), with thiophene derivatives such as thieno[3,2-b]thiophene and 2,2′-bithiophene as a donor and thiophene containing different conjugated side-groups as an acceptor. To enhance the absorption region of these polymers, DTBT and DPP as electron-accepting groups are adopted into the side-groups. We attached alkoxy and branched 2-ethylhexyl groups on the acceptor to promote the solubility of the resulting polymers. The conjugated side-chain groups were connected to the main-chain using the 2-vinylene group. The vinylene connector eliminates torsional strains between the main-chain and electron-accepting side-chain. It helps to extend the π-conjugation and improve the coplanarity of the polymer backbone, leading to a reduced optical bandgap and adjustable energy levels of frontier molecular orbital. The effects of the conjugated side chains on the thermal, photophysical, electrochemical, and photovoltaic properties of the copolymers were also researched specifically. Lastly, the distribution rate and contact between the 2D D–A copolymers with conjugated side-chain and $PC_{70}BM$ in an active layer were investigated to determine the mechanism of their interaction.

EXPERIMENTAL

Materials

2,5-bis(trimethylstannyl)thieno[3,2-b]thiophene(D1) and all starting materials were purchased the TCI, Sigma Aldrich, and Alfar Aesar companies. And the materials were used without further purification. THF, ether, toluene were distilled before use. The 2,5-*bis*(trimethylstannyl)−2,2′-bithiophene(D2),[26] 5,6-*bis*(octyloxy)−4,7-dithien-2-yl-benzo[c][1,2,5]thiadiazole(1),[27] 2,5-*bis*(2-ethylhexyl)−3,6-dithien-2-yl-pyrrolo[3,4-c]pyrrole-1,4(2H,5H)-dione (2),[28] diethyl-2-(2,5-dibromothiophen-3-yl)ethyl phosphonate(3)[29] were synthesized modified procedures according to the reported procedures.

5-(5,6-*Bis*(octyloxy)-7-(thien-2-yl)benzo[c][1,2,5] thiadiazol-4-yl)thien-2-carbaldehyde (4)

Anhydrous DMF (0.8 mL, 10.2 mmol) was added dropwise to a solution of 1 (5.68 g, 10.2 mmol) in $C_2H_4Cl_2$ (50 mL) under the nitrogen, then $POCl_3$ (0.96 mL, 10.2 mmol) was added slowly at 0 °C. The mixture was heated and stirred at

85 °C for 12 h. After cooling to room temperature (RT), 60 mL water was added to end the reaction. The mixture was extracted with CH_2Cl_2. After the solvent was distilled, the residue was purified by silica gel chromatography using petroleum ether:dichloromethane (1:1) as eluent. 4 was obtained an orange solid (Yield: 4.24 g, 71%). ^{1}H-NMR (400 MHz, $CDCl_3$, δ): 9.84 (s, 1H), 8.47 (d, 1H, J = 4.0 Hz), 8.37 (d, 1H, J = 1.2 Hz), 7.65 (d, 1H, J = 4.0 Hz), 7.38 (d, 1H, J = 4.0 Hz), 7.08 (d, 1H, J = 3.6 Hz), 4.00 (t, 4H, J = 7.2 Hz), 1.86–1.79 (m, 4H), 1.31 (m, 5H), 1.22–1.18 (m, 17H), 0.80–0.76 (m, 6H). ^{13}C-NMR (400 MHz, $CDCl_3$, δ): 183.4, 153.6, 151.3, 150.6, 143.5, 135.7, 133.7, 131.2, 128.1, 126.7, 119.5, 116.0, 74.6, 31.87, 30.38, 29.5, 29.33, 26.0, 22.7, 14.17. Anal. calcd. for $C_{31}H_{40}N_2O_3S_3$: C, 63.66; H, 6.89; N, 4.79; O, 8.21; S, 16.45. Found: C, 63.78; H, 6.84; N, 4.75; O, 8.19; S, 16.44. GC/MS ($C_{31}H_{40}N_2O_3S_3$) m/z: calcd. for 584.22; found 584.24.

5-(2,5-*Bis*(2-ethylhexyl)-3,6-dioxo-4-(thien-2-yl)-2,3,5,6-tetrahydropyrrolo[3,4-c]pyrrol-1-yl)thien-2-carbaldehyde (5)

Material 5 was synthesized with the same procedure of 4. To solution of 2 (1.04, 10.20 mmol) in $C_2H_4Cl_2$, anhydrous DMF (0.8 mL, 10.2 mmol) was added dropwise. Then, $POCl_3$ (0.96 mL, 10.2 mmol) was added slowly. The mixture was heated and stirred at 85 °C for 12 h. After cooling to RT, water was poured into the mixture and extracted with chloroform. The organic layer was removed the solvent, and the crude product was purified using silica gel chromatography (eluent: DCM:PE = 1:1 to 1:0). 5 was obtained a purple solid (0.27 g, 49%). ^{1}H-NMR (400 MHz, $CDCl_3$, δ): 10.01 (s, 1H), 9.06 (t, J = 2.0 Hz, 1H), 8.94 (d, J = 4.0 Hz, 1H), 7.86 (d, J = 4.0 Hz, 1H), 7.71(t, J = 2.4 Hz, 1H), 7.31 (d, J = 1.2 Hz, 1H), 4.05 (t, J = 3.8 Hz, 4H), 1.88–1.83 (m, 2H), 1.36–1.24 (m, 17H), 0.88–0.85 (m, 13H). ^{13}C-NMR (400 MHz, $CDCl_3$, δ): 182.8, 161.9, 161.3, 145.5, 142.9, 137.7, 136.5, 134.9, 132.0, 129.5, 128.8, 110.9, 108.1, 46.0, 39.3, 39.1, 30.2, 30.1, 28.3, 23.5, 23.1, 14.0, 10.5. Anal. calcd. for $C_{15}H_6N_2O_3S_2$: C, 55.20; H, 1.85; N, 8.58; O, 14.71; S, 19.65. Found: C, 55.16; H, 1.83; N, 8.59; O, 14.69; S, 19.73. GC/MS ($C_{15}H_6N_2O_3S_2$) m/z: calcd. for 325.98; found 326.08.

(E)-4-(5-(2-(2,5-dibromothiophen-3-yl)vinyl)thien-2-yl)-5,6-*bis*(octyloxy)-7-(thien-2-yl)benzo[c][1,2,5]thiadiazole (A1)

Under a nitrogen atmosphere, a solution of 3 (1.21 g, 3.2 mmol) and 4 (1.87 g, 3.2 mmol) in THF (30 mL) was stirred and degassed for 0.5 h at RT. Then mixture of potassium tertbutoxide (0.672 g, 6.0 mmol) in THF (20 mL) was added dropwise into it. The reaction mixture was stirred at RT for 8 h, and then refluxed at 60 °C for 12 h. After cooling to RT, the reaction mixture was extracted with CH_2Cl_2 and washed with dilute aqueous HCl solution, water. The organic layer was dehydrated using anhydrous $MgSO_4$, and the solvent was distilled by rotary evaporation. By silica gel chromatography, the residue was purified using a hexane/CH_2Cl_2 mixture (1:1 by volume) as eluent. A red solid was obtained. Yield: 2.564 g (97%). ^{1}H-NMR (400 MHz, $CDCl_3$, δ): 8.48 (s, 2H), 7.50 (d, J = 4.8 Hz, 1H), 7.23 (t, J = 5.6 Hz, 2H), 7.19 (s, 1H), 7.06 (d, J = 16 Hz, 1H), 6.90 (d, J = 16 Hz, 1H), 4.145 (m, 4H), 1.98-1.93 (m, 4H), 1.50–1.45 (m, 4H), 1.32–1.28 (m, 18H), 0.89–0.85 (m, 6H). ^{13}C-NMR (400 MHz, $CDCl_3$, δ): 150.8, 149.7, 141.9, 137.9, 133.0, 130.4, 129.6, 126.2, 125.8, 123.4, 118.6, 116.7, 116.2, 110.9, 108.8, 73.4, 30.8, 29.5, 28.7, 28.5, 28.3, 25.0, 21.7, 13.1. Anal. calcd. for $C_{36}H_{42}Br_2N_2O_2S_4$: C, 52.55; H, 5.15; Br, 19.42; N, 3.40; O, 3.89; S, 15.59. Found: C, 52.53; H, 5.08; Br, 19.46; N, 3.39; O, 3.85; S, 15.69. GC/MS ($C_{36}H_{42}Br_2N_2O_2S_4$) m/z: calcd. for 822.05; found 821.95.

(E)-3-(5-(2-(2,5-dibromothiophen-3-yl)vinyl)thien-2-yl)-2,5-*bis*(2-ethylhexyl)-6-(thien-2-yl)pyrrolo[3,4-c]pyrrole-1,4(2H,5H)-dione (A2)

A2 was synthesized with the same procedure of A1. Under a nitrogen atmosphere, a solution of 3 (1.42 g, 3.62 mmol) and 5 (2.0 g, 3.62 mmol) in THF (36 mL) was stirred and degassed for 0.5 h at RT. Then mixture of potassium tertbutoxide (0.812 g, 7.24 mmol) in THF (24 mL) was dropwised to the solution and stirred at RT for 8 h. The mixture refluxed at 60 °C for 12 h. After cooling to RT, the mixture was extracted with CH_2Cl_2 and washed with dilute HCl aqueous solution, water. The organic layer was dehydrated using anhydrous $MgSO_4$ and the solvent was distilled by rotary evaporation. By silica gel chromatography, the crude product was purified using hexane: CH_2Cl_2 (3:1) as eluent. A purple solid was obtained. Yield: 2.5 g (70%). ^{1}H-NMR (400 MHz, $CDCl_3$, δ): 8.94 (t, J = 4.6 Hz, 2H), 7.62 (t, J = 2.4 Hz, 1H), 7.27 (d, J = 2.4 Hz, 1H), 7.22 (t, J = 9.0 Hz, 2H), 7.04 (d, J = 16 Hz, 1H), 6.92 (d, J = 16 Hz, 1H), 4.03 (m, 4H), 1.59 (m, 2H), 1.37–1.26 (m, 17H), 0.92–0.86 (m, 12H). ^{13}C-NMR (400 MHz, $CDCl_3$, δ): 161.7, 147.1, 140.1, 139.8, 138.3, 136.6, 135.4, 130.6, 129.9, 128.4, 128.0, 127.1, 123.3, 121.9, 112.4, 108.2, 45.93, 39.2, 30.23, 28.4, 23.6, 23.1, 14.1, 10.6. Anal. calcd. for $C_{20}H_8Br_2N_2O_2S_3$: C, 42.57; H, 1.43; Br, 28.32; N, 4.96; O, 5.67; S, 17.05. Found: C, 42.52; H, 1.48; Br, 28.38; N, 4.92; O, 5.63; S, 17.07. GC/MS ($C_{20}H_8Br_2N_2O_2S_3$) m/z: calcd. for 563.81; found 563.87.

General Polymerizations

To a mixture of *tris*(dibenzylideneacetone)dipalladium(0) (Pd_2dba_3) (7.3 mg, 0.008 mmol, 2.7 mol %), tri-(*o*-tolyl)-phosphine (9.7 mg, 0.032 mmol, 10.7 mol %), stannane compound (0.2 mmol, e.g., D1 and D2) and equal halogen compound (e.g., A1 and A2) were dissolved in 8 mL of anhydrous toluene. Under the nitrogen, the mixture was powerfully stirred and refluxed at 90–95 °C for 48 h. 2-bromotihophene was added to the reaction after 48 h. And after 3 h, 2-trimethylstannyl thiophene was added to end-capping reaction. After cooling the mixture to RT, it was put into methanol and filtered. The filtered precipitate was reprecipitated after dissolving in $CHCl_3$, dropping into methanol and then filtered. The polymer was further purified by Soxhlet extraction using methanol, acetone, $CHCl_3$, and *o*-dichlorobenzene, respectively for 24 h. The chloroform part was reprecipitated with methanol, then filtrated, and desiccated under reduced pressure at 50 °C.

Poly[2,5-thieno[3,2-b]thiophene-alt-(E)-4-(5-(2-thien-3-yl)vinyl)thien-2-yl)-5,6-*bis*(octyloxy)-7-(thien-2-yl)benzo[c][1,2,5]thiadiazole] (PfToBT)

Dark black purple solid, 0.150 g (yield = 62%). ^{1}H-NMR (400 MHz, $CDCl_3$, δ): δ 8.47 (m, 3H), 7.40 (m, 4H), 7.15 (m, 3H) 4.11 (m, 4H), 1.88–1.83 (m, 6H), 1.25 (2, 19H), 0.84–0.81 (m, 9H). Anal. calcd. for $C_{42}H_{44}N_2O_2S_6$: C, 63.57; H, 6.06; N, 3.37; O, 3.85; S, 23.14. Found: C, 64.04; H, 7.47; N, 2.45; O, 2.84; S, 23.2

Poly[2,2'-bithiophene-alt-(E)-4-(5-(2-thien-3-yl)vinyl)thien-2-yl)-5,6-*bis*(octyloxy)-7-(thien-2-yl)benzo[c][1,2,5]thiadiazole] (PbToBT)

Dark black purple solid, 0.165 g (yield = 66%). ^{1}H-NMR (400 MHz, $CDCl_3$, δ): δ 8.44 (m, 4H), 7.52–7.40 (m, 4H), 7.15 (m, 3H) 4.09 (m, 4H), 1.92 (m, 7H), 1.25 (s, 21H), 0.86–0.85 (m, 9H). Anal. calcd. for $C_{44}H_{46}N_2O_2S_6$: C, 64.45; H, 6.11; N, 3.27; O, 3.73; S, 22.44. Found: C, 66.2; H, 7.27; N, 3.04; O, 3.44; S, 23.49

Poly[2,5-thieno[3,2-b]thiophene-alt-(E)-3-(5-(2-(thien-3-yl)vinyl)thien-2-yl)-2,5-*bis*(2-ethylhexyl)-6-(thien-2-yl)pyrrolo[3,4-c]pyrole-1,4(2H,5H) -dione] (PfTDPP)

Dark black purple solid, 0.200 g (yield = 86%). ^{1}H-NMR (400 MHz, $CDCl_3$, δ): δ 8.89 (m, 3H), 7.73–7.44 (m, 4H), 7.01 (m, 3H) 4.03 (m, 4H), 1.85 (m, 3H), 1.25 (m, 16H), 0.87 (m, 8H). Anal. calcd. for $C_{41}H_{44}N_2O_2S_5$: C, 66.12; H, 6.31; N, 3.51; O, 4.00; S, 20.06. Found: C, 67.3; H, 6.59; N, 3.25; O, 3.86; S, 19.0

Poly[2,2'-bithiophene-alt-(E)-3-(5-(2-(thien-3-yl)vinyl)thien-2-yl)-2,5-*bis*(2-ethylhexyl)-6-(thien-2-yl)pyrrolo[3,4-c]pyrrole-1,4(2H,5H)-dione] (PbTDPP)

Dark black purple solid, 0.180 g (yield = 75%). ^{1}H-NMR (400 MHz, $CDCl_3$, δ): δ 8.90 (m, 4H), 7.52–7.31 (m, 4H), 7.02 (m, 4H) 4.00 (m, 4H), 2.04$\sim$1.85 (m, 5H), 1.25 (m, 17H), 0.87 (m, 11H). Anal. calcd. for $C_{43}H_{46}N_2O_2S_5$: C, 66.95; H, 6.35; N, 3.39; O, 3.88; S, 19.43. Found: C, 66.94; H, 6.57; N, 3.29; O, 3.84; S, 19.36

Measurements

^{1}H- and ^{13}C-NMR data were performed on a Brüker AMX400 spectrometer in $CDCl_3$. And TMS as the internal standard in $CDCl_3$ calibrated the chemical shifts indicated in measures of ppm. The Ultraviolet–visible (UV–vis) absorption spectra were carried out on an Agilent 8453 UV–visible spectroscopy system. The solutions used for experiments of the UV–visible absorption spectra were dissolved in $CHCl_3$ at various concentrations. The films were drop-coated from the 1 mg/mL solution on a quartz substrate. The molecular weight and polydispersity index (PDI) of the polymers were determined by gel permeation chromatography (GPC) analyses using THF as the eluent and a polystyrene standard as the reference. The thermal analyses were recorded using a TG 209 F3 thermogravimetric analyzer (TGA) under a N_2 atmosphere. The cyclic voltammetry (CV) was recorded in solid-state using a Zahner IM6eX electrochemical workstation with three electrodes system in a 0.1M tetrabutylammonium hexafluorophosphate (Bu_4NPF_6) acetonitrile solution: working electrode = the polymer film on a ITO glass, counter electrode = a ITO glass, and reference electrode = silver/silver chloride [Ag in 0.1M KCl]. The constant scan rate was 50 mV/s. The electrochemical potential was calibrated against Fc/Fc^+. X-ray diffraction (XRD) patterns was performed using a New D8-Advance instrument of Bruker-AXS and SmartLab 3kW (40 kV 30 mA, Cu target) of Rigaku. Thicknesses of the active layers were recorded by a KLA Tencor Alpha-step 500 surface profilometer. The depth profile of the blend film was detected by X-ray photoelectron spectroscopy (XPS) measurement which was performed from PHI 5000 VersaProbe ll system with a microfocused (100 mm, 25 W) Al X-ray beam during *in situ* sputtering. In brief, the Ar+ ion beam was created from Ar^+ ion source (Fig-5CE $\geq$5.0 μA at 5 kV). Using turbomolecular and ion-getter pumps, the measurement was accomplished at the pressure of $<1 \times 10^{-7}$ Pa by evacuating the main chamber. The current density–voltage (J–V) curves of the PSCs were performed by Keithley 2400 source measurement unit (SMU) furnished with a Class A Oriel solar simulator under an AM 1.5G illumination, 100 mW/cm^2. To obtain topographic images of the active layers, atomic force microscopy (AFM) in tapping mode was performed by an XE-100 instrument under ambient conditions.

Photovoltaic Cell Fabrication and Treatment

The photovoltaic cells were constructed in the following conventional structure of ITO (170 nm)/PEDOT:PSS (30 nm)/polymer:$PC_{70}BM$/BaF_2 (1 nm)/Ba (2 nm)/Al (200 nm). The patterned indium tin oxide (ITO) glass [Sanyo, Japan(10 Ω/γ)] was cleaned with detergent, deionized water, acetone, and isopropyl alcohol in ultrasonicator. It dried at 120 °C for 10 min on a hot plate and treated with ultraviolet–ozone chamber for 10 min.

Poly(3,4-ethylene-dioxythiophene):poly(styrene sulfonate) (PEDOT:PSS, Baytron P 4083 Bayer AG) was filtered through a 0.45-mm filter and spin-coated on cleaned-ITO at 4000 rpm in air. Then, substrate was dried at 120 °C for 20 min and transferred to a N_2-filled glove box. An *o*-dichlorobenzene solutions of the polymers and 1-(3-methoxycarbonyl)propyl-1-phenyl-[6,6]-C71($PC_{70}BM$) blended in 1:2 (w/w) and 1:3 (w/w) were spin-coated (500–3000 rpm, 30 s) on to the PEDOT:PSS layer. The substrates with the spin-casted active layer films were dried for 10 min at 120 °C inside a glove box. BaF_2 (1 nm) and Ba (2 nm) were then deposited as an electron injection cathode on to the active layer. The device was completed by depositing of 200-nm aluminum layer using thermal evaporator at pressures lower than 10^{-6} Torr. The yielded devices had an active area of 4 mm^2. Finally, the devices were encapsulated using a UV-curable epoxy (Nagase, Japan) and glass slide.

The single-carrier diodes were fabricated based on a configuration of ITO (170 nm)/PEDOT:PSS (40 nm)/Polymer:$PC_{70}BM$/MoO_3 (30 nm)/Al (100 nm) for calculating hole mobility. The hole mobilities of the active layers were extracted from the J–V graphs of the hole-only devices

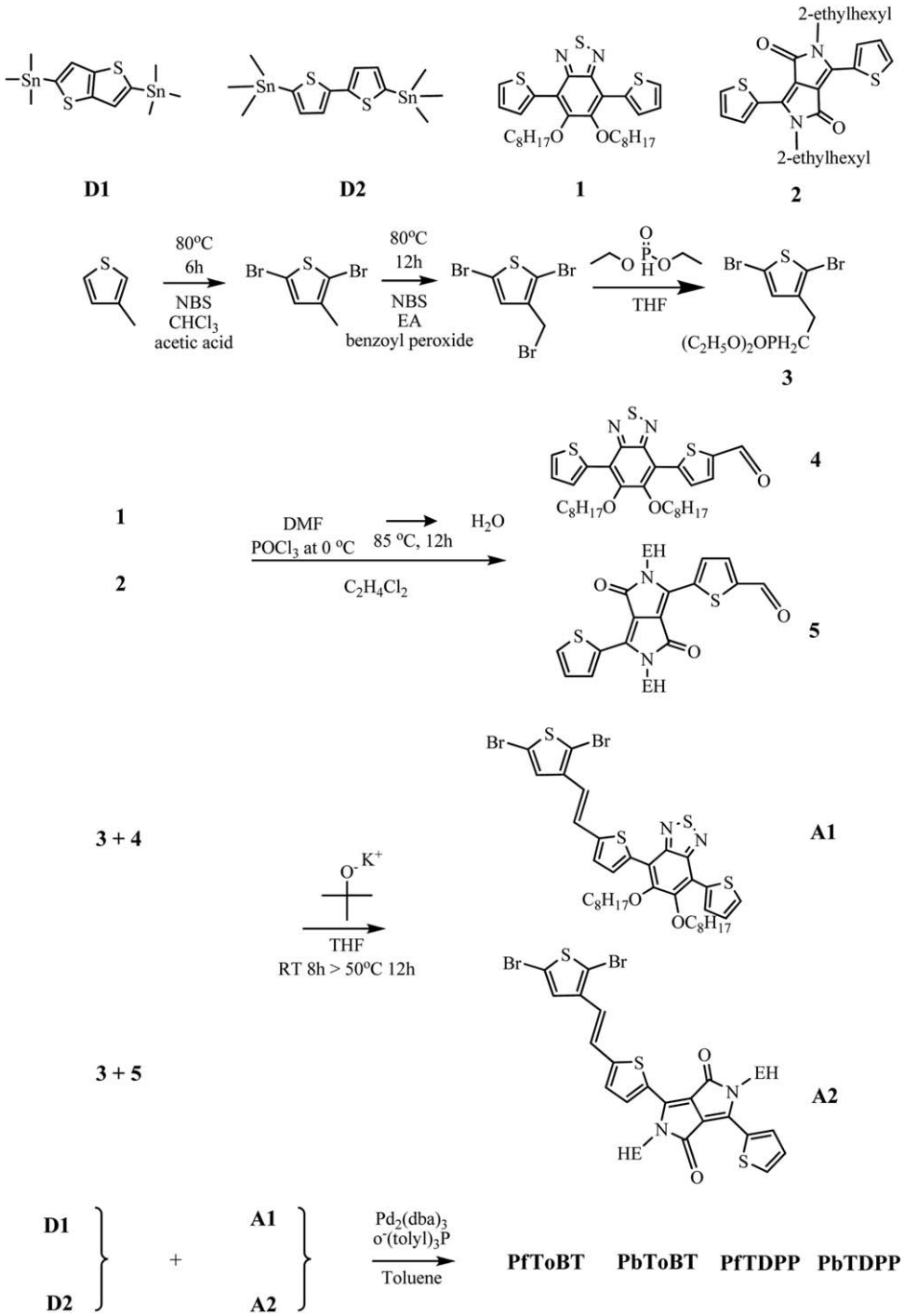

SCHEME 1 Synthetic route to monomers and polymers.

recorded in the dark conditions. The Mott–Gurney equation is as follow:

$$J=\frac{9}{8}\varepsilon\varepsilon_0\mu_{h(e)}\frac{V^2}{L^3}\exp(0.89)\gamma\sqrt{\frac{V}{L}}$$

where ε_0 (8.85×10^{-14} F/cm) is the permittivity of vacuum; ε is the permittivity of the polymer:$PC_{70}BM$ blend; μ is the mobility; L is the thickness of the thin film; and V is the voltage ($V_{bi} - V_r + V_{appl}$), where V_{bi} is the built-in voltage; V_r is the voltage drop because of series resistance across the electrodes; V_{appl} is the applied voltage to the device.

RESULTS AND DISCUSSION

Synthesis and Characterization of Polymers

Scheme 1 and Figure 1 showed the copolymer structures and common methods of synthesis. Compound 3 was

TABLE 1 Polymerization Results and Degradation Temperatures of Polymers

Polymer	Yield (%)	Mn[a] (kDa)	Mw[a] (kDa)	PDI[a]	Degree of Polymerization	T_d (°C)
PfToBT	62	60	281	4.6	72	390
PbToBT	66	85	348	4.1	99	394
PfTDPP	86	66	220	3.3	83	382
PbTDPP	75	82	272	3.3	100	344

[a] Indicated by solution in $CHCl_3$ using GPC. Calibrated by polystyrene standards.

synthesized by starting with the bromination of 3-methylthiophene using NBS at 80 °C, which afforded 2,5-dibromo-3-methylthiophene. Then bromination of 2,5-dibromo-3-methylthiophene in ethylacetate yielded 2,5-dibromo-3-bromomethylthiophene. Compound 3 was synthesized from 2,5-dibromo-3-bromomethylthiophene by the Wittig–Horner reaction. Compounds 4 and 5 were prepared from compounds 1 and 2 using the Vilsmeier–Haack reaction. A1 and A2 were then prepared from compound 3 and aldehyde-containing materials (Compounds 4 and 5) in average yields according to the Wittig–Horner reaction[30] for the resulting copolymers PfToBT, PbToBT, PfTDPP, and PbTDPP using a Stille coupling reaction with D1 and D2. The structures of the synthesized monomers and polymers were confirmed using ^1H, ^{13}C-NMR (as shown in Supporting Information Figs. S1–S9) and elemental analysis (EA). PfTDPP and PbTDPP exhibit good solubility in common organic solvents such as tetrahydrofuran (THF), chloroform ($CHCl_3$), *o*-dichlorobenzene (*o*-DCB), and chlorobenzene (CB). Conversely, PfToBT and PbToBT are not soluble in these solvents at RT and are soluble only at elevated temperature.

The measured polymer molecular weights and thermal properties are summarized in Table 1. PfToBT, PbToBT, PfTDPP, and PbTDPP have molecular weights (Mw) of 281, 348, 220, and 272 kDa, respectively, and broad PDI of 4.6, 4.1, 3.3, and 3.3, respectively. These data were indicated using GPC, calibrated by polystyrene standards with $CHCl_3$ base. As listed in Table 1, the molecular weights of PbToBT and PbTDPP are higher than PfToBT and PfTDPP, presumably due to bithiophene donor unit that release the diheral angle. This decrease of steric hindrance directly impacts the polymer molecular weight, a dominant factor in determining the chain packing and mechanical properties of polymer thin films.[31] To compare 2D-conjugated polymers with CT-type polymers which have similar chemical structures, the molecular weight of the four copolymers is relatively higher, and the PDI is broader.[32–35] The vinylene linkage eliminates torsional strains between the main-chain and electron-accepting side-chain. So it can help to extend the π-conjugation and improve the coplanarity of the polymer backbone. The Mw and PDI are affected by the polymerization conditions (i.e., the purity of the monomers and the solubility of the monomers and polymers).[16] Moreover, the degree of polymerization may also be influenced the high degree of planarity of PfToBT, PbToBT, PfTDPP, and PbTDPP's main backbone consisting of only thiophene derivatives, which in turn may have an impact on the photovoltaic performances.

The thermal weight loss in nitrogen atmosphere of the copolymers was performed by TGA at 20 °C min^{-1} heating rate. All of the synthesized polymers (PfToBT, PbToBT, PfTDPP, and PbTDPP) exhibited superior thermal stability with onset degradation temperatures (T_d) of a 5% weight-loss from 344 to 394 °C, as shown in Supporting Information Figure S10. The obtained copolymers had adequate thermal stability, which proved to be suitable for application in optoelectronics and device fabrication.

Optical Properties

The UV–visible absorption of all copolymers in solution and thin film was investigated. The correlative data of the copolymers are summarized in Figure 2 and Table 2. Figures 2(a) and Supporting Information Figure S11 indicate the UV–vis absorption spectra of PfToBT, PbToBT, PfTDPP, and PbTDPP in diluted $CHCl_3$ solutions at various concentrations and calculation of molar absorption coefficients (ε). The copolymers show three distinct absorption peaks. The first peak around 311–343 nm is caused by the n–π^* absorption of the DPP or the 5,6-*bis*(octyloxy)−4,7-di(thien-2-yl)benzo[c][1,2,5]thiadiazole (DToBT) group.[36] The second peak with the absorption maxima($\lambda_{s,\ max}$) at 388 nm for PfToBT, 388 nm for PbToBT, 408 nm for PfTDPP, and 408 nm for PbTDPP is caused by the π–π^* transition of the delocalized excitons. Whereas the third peak at 501, 502, 560, and 564 nm, respectively, can be identified to a localized intramolecular transition between donor and acceptor.[37] PfTDPP and PbTDPP exhibit a little wider absorption region which is resulted from the intramolecular charge transfer (ICT) interaction between the polymer backbone and the conjugated side chain.[38] Evidently, the ICT interactions of PfTDPP and PbTDPP are gradually increased because of the stronger electron-withdrawing ability of the DPP of A2 than DToBT of A1. The calculated absorption coefficients of PfToBT, PbToBT, PfTDPP, and PbTDPP are 3.64, 4.00, 5.03, and 6.28 $\times$ 10^4 $(g\ mL^{-1})^{-1}$ cm^{-1}, respectively at $\lambda_{s,max}$.

The absorption coefficients of PfTDPP and PbTDPP are higher than those of PfToBT and PbToBT, because of the introduction of brilliant red dye (in DPP unit) to the side group. These results convincingly demonstrate that DPP-containing polymers (PfTDPP and PbTDPP) have better light-

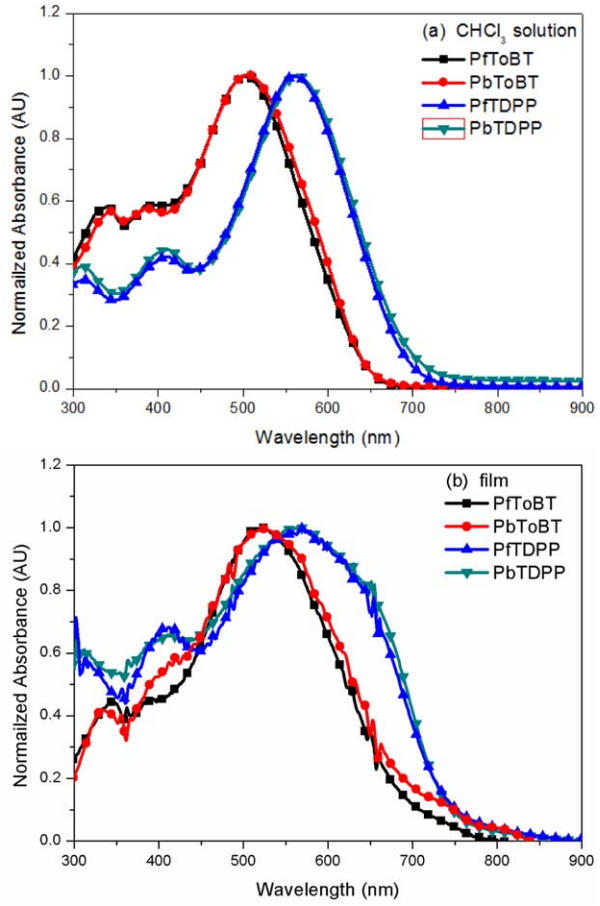

FIGURE 2 Normalized UV–vis absorption spectra of copolymers: (a) in solution and (b) film. [Color figure can be viewed in the online issue, which is available at wileyonlinelibrary.com.]

harvesting ability than DToBT-containing polymers (PfToBT and PbToBT) indicating that the former can give a higher Jsc than the latter.[13] As shown in Figure 2(b), the absorption peaks of all copolymers in the films were red-shifted compared to those in solution. This characteristics may be accounted for the improved aggregation and interchain interaction of the polymer backbones in solid state, which is likely associated with the increased polarizability and extent of π–π stacking of the polymers.[39] The optical bandgaps (E_g^{opt}) of PfToBT, PbToBT, PfTDPP, and PbTDPP are 1.79, 1.78, 1.68, and 1.66 eV, respectively, inferred from the edge of the absorptions in film. Compared to the parent polymers (PPDToBT, PABToBT, DPPT-TT, and pBBTDPP2) which have linear CT-type structure with similar donor and acceptor units, the narrow absorptions of the graft structure copolymers PfToBT, PbToBT, PfTDPP, and PbTDPP are observed from 300 to 800 nm. The observed blue-shifted absorption phenomenon are related to weaker D-A interaction in the graft-type copolymer compared to linear-type copolymer.[40] These results clearly indicate that introducing different conjugated side-groups can control the optical properties of these 2D polymers.[16]

Electrochemical Measurements and Computational Study of Polymers

Cyclic voltammetry (CV) was produced to investigate electrochemical behavior of the copolymers.

The results data of corresponding with CV curves are presented in Figure 3 and summarized in Table 2. Redox potentials were calibrated by using the ferrocene/ferrocenium(Fc/Fc^+) redox couple as the internal standard. The redox potential of Fc/Fc^+ is assumed 0.43 V versus Ag/AgCl, which have a definite vacuum energy level of 4.8 eV.

The oxidation onset potentials (E_{ox}) for PfToBT, PbToBT, PfTDPP, and PbTDPP are 0.97, 0.95, 0.83, and 0.75 V, respectively. The calculated HOMO levels are at −5.34, −5.32, −5.23, and −5.12 eV for PfToBT, PbToBT, PfTDPP, and PbTDPP, respectively. The copolymers have lower HOMO levels than air oxidation threshold (−5.20 eV). PfToBT, PbToBT, and PfTDPP are expected to have good oxidative stability.[16] Introducing benzothiadiazole(BT) unit to the backbone contributes to the relatively lower HOMO energy levels of PfToBT and PbToBT compared with PfTDPP and PbTDPP due to the BT unit has a lower HOMO level than the DPP unit. This result is in agreement with that obtained by You et al. regarding the HOMO level of a polymer containing BT, which has a side-chain in its core.[41] The HOMO energy level is primarily determined by the donor unit in the type of a D–A

TABLE 2 Photophysical and Electrochemical Measurements of Polymers

Polymer	UV–Vis Absorption				Cyclic Voltammetry		
	$CHCl_3$ Solution	Film		$E_g^{op,a}$ (eV)	E_{ox}^{onset} (V)	HOMO[b] (eV)	LUMO[b] (eV)
	$\lambda_{s,max}$ (nm)	$\lambda_{f,max}$ (nm)	λ_{onset} (nm)				
PfToBT	340, 388, 501	346, 390, 524	693	1.79	0.97	−5.34	−3.55
PbToBT	343, 388, 502	334, 411, 525	694	1.78	0.95	−5.32	−3.54
PfTDPP	311, 408, 560	312, 412, 569	738	1.68	0.83	−5.23	−3.52
PbTDPP	312, 408, 564	312, 411, 571	747	1.66	0.75	−5.12	−3.46

[a] From the absorption spectrum of film state, E_g^{op} calculated from the point of contact with the baseline and the tangent on the low energetic edge.

[b] $E_{HOMO\ (or\ LUMO)} = -e[E_{onset}(\text{vs. Ag/AgCl}) - E_{1/2}(Fc/Fc^+ \text{ vs. Ag/AgCl})] - 4.8$ eV.

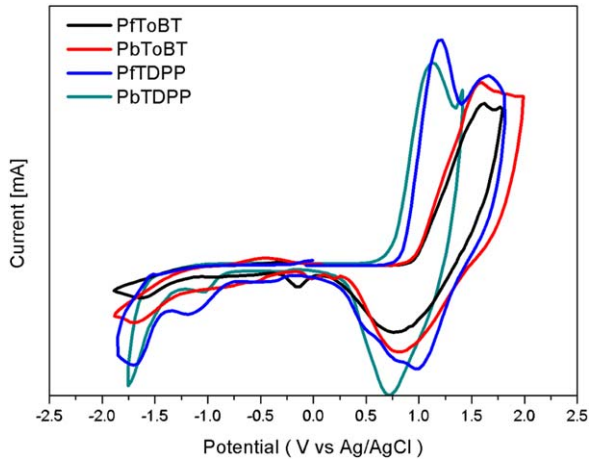

FIGURE 3 Cyclic voltammograms of polymers. [Color figure can be viewed in the online issue, which is available at wileyonlinelibrary.com.]

copolymer. Also the HOMO levels of PfToBT and PfTDPP are slightly deeper than those of PbToBT and PbTDPP because the HOMO energy level of the thieno[3,2-b]thiophene electron-donating unit of PfToBT and PfTDPP is relatively lower than the bithiophene electron-donating unit of PbToBT and PbTDPP.[42] The PfToBT and PbToBT with same conjugated side chains have a similar HOMO level. So we expected that they would show a similar Voc value to the resulting PSCs. As PfToBT and PbToBT have deep-lying HOMO levels, these PSCs would have high V_{OC} values. The fact, value of Voc in BHJ PSCs is directly proportional to the difference between the HOMO level of the p-type and the LUMO level of the n-type, has been demonstrated. In addition, the LUMO levels are −3.55, −3.54, −3.52, and −3.46 eV for PfToBT, PbToBT, PfTDPP, and PbTDPP, respectively. The energy differences of the LUMO levels are higher than 0.3 eV to yield sufficient exciton dissociation and efficient charge transfer when comparing LUMO levels of the copolymers with those of the acceptor ($PC_{70}BM = -4.3$ eV).[43]

To gain a understanding of the electron density of states distribution and electronic properties, as well as the molecular geometries of the polymers with different side-groups, simulations were performed using density functional theory (DFT). Computation was performed at the B3LYP/6-31G(*d*) with Gaussian 09, which is suitable program for using theoretical calculations. For the purpose of computational simplification, two repeating units were selected to the polymer backbones. Figure 4 shows the molecular orbitals of calculated HOMO and LUMO. The data of these calculations are summarized in Table 3. DPP has greater electron-withdrawing capability as an acceptor than oBT, which is reflected in the shapes of electron density of these HOMO and LUMO orbitals. The HOMOs and LUMOs are localized on oBT and DPP unit as the acceptor. This is because of the features of the quinoid structure built between the nonbonding electron pairs of nitrogen and sulfur, which have electron-accepting characteristics.[44] In the case of PfToBT and

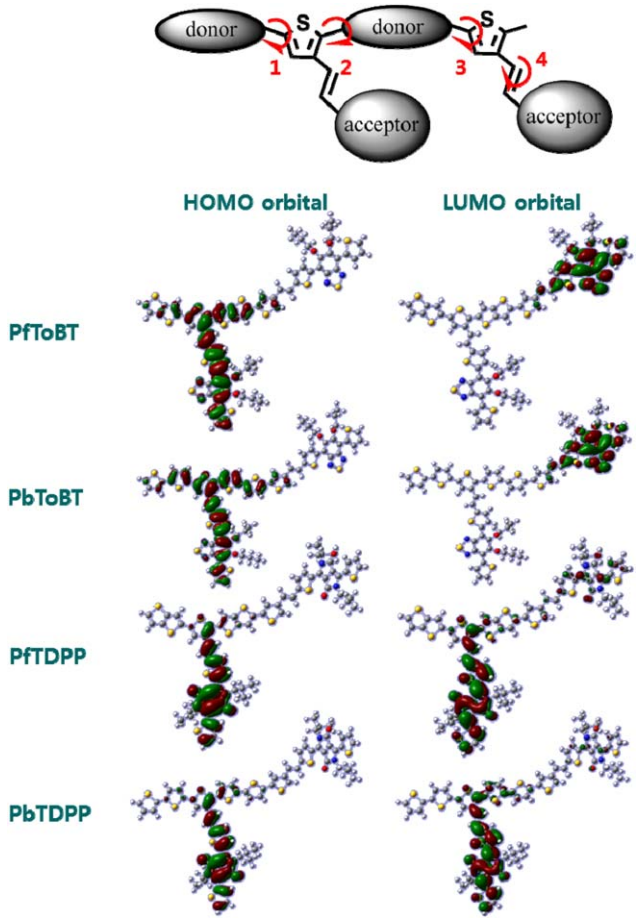

FIGURE 4 The frontier molecular orbitals for polymer dimer models. [Color figure can be viewed in the online issue, which is available at wileyonlinelibrary.com.]

PbToBT, the electrons are distributed primarily on the oBT side group with a small distribution on the thiophene donor groups (HOMO). The LUMO is spread out on the oBT side-group only, which allows the external excitations are able to electron transfer from the left to right side in molecules. The distribution of the HOMO electron density of PfTDPP and PbTDPP is weighted more towards the accepting side group than in PfToBT and PbToBT because DPP is better electron acceptor than oBT.

As shown in Table 3, the HOMO levels determined from the DFT calculations tend to increase using the bithiophene

TABLE 3 Theoretical Data of Polymers

Polymer	Dihedral Angle (°) 1	2	3	4	$HOMO^{cal.}$ (eV)	$LUMO^{cal.}$ (eV)
PfToBT	0.76	46.65	1.59	36.26	−7.119	0.438
PbToBT	0.41	50.71	0.31	35.49	−7.050	0.446
PfTDPP	1.63	46.01	1.57	45.86	−6.958	0.356
PbTDPP	1.48	49.50	0.28	42.81	−6.934	0.368

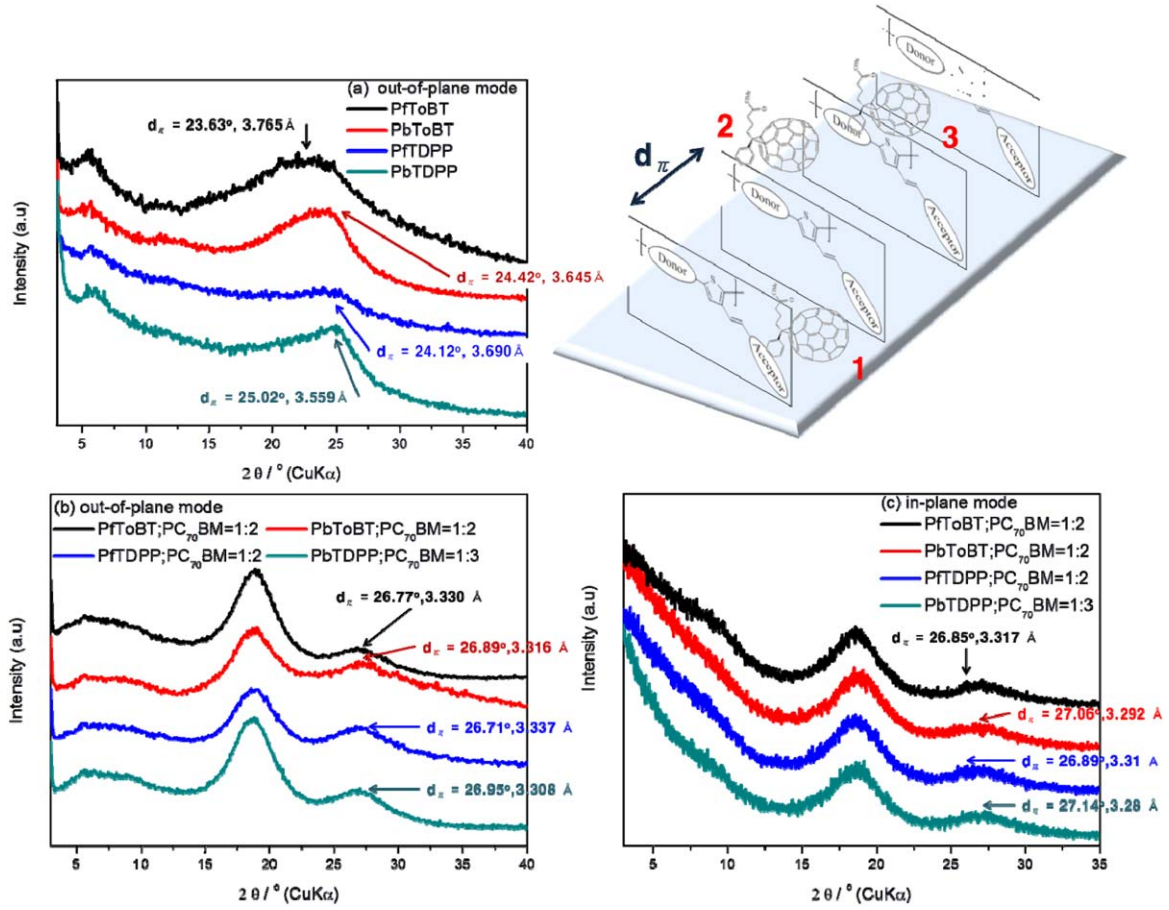

FIGURE 5 X-ray measurements data with thermally annealed thin films of polymers and polymer:$PC_{70}BM$ blend on silicon wafer: (a), (b), out-of-plane mode and (c) inplane mode. [Color figure can be viewed in the online issue, which is available at wileyonlinelibrary.com.]

donor or DPP derivative on the polymer backbone. This agrees with the CV measurements in which strengthen of the electron-donating ability of the donor unit makes the HOMO level increases. Moreover, the dihedral angles 1, 2, 3, and 4 between the donor unit, vinyl thiophene and side groups (summarized in Table 3) demonstrate similar values for each of the four polymers. The dihedral angles 1, 3, and 4 (0.41°/0.31°/35.49°, and 1.48°/0.28°/42.81°) of the polymers with bithiophene donor (PbToBT and PbTDPP, respectively) are observed to be smaller than those (0.76°/1.59°/36.26° and 1.63°/1.57°/45.86°) of the polymers with the fused thiophene donor (PfToBT and PfTDPP, respectively). Therefore, the structure and planarity of the donor unit plays a decisive role in determining the HOMO energy level. In the case of PbToBT and PbTDPP, the introduction of the bithiophene extends the conjugation in the polymer main chains. This increases the electron-donating activity of PbToBT and PbTDPP and results in the increased HOMO levels.

XRD Measurements

To gain a better understanding of the ordering and orientation in thin films of the graft-structure polymers, X-ray diffraction (XRD) measurements were performed with their associated annealing temperatures. XRD diffraction patterns of the polymer pristine films acquired in the out-of-plane mode were shown in Figure 5(a) to analyze the arrangement structure. PfToBT, PbToBT, PfTDPP, and PbTDPP thin films, obtained in the out-of-plane mode, showed small diffraction peaks for the (100) planes and broad diffraction peaks for the (010) crystal planes. This suggests that the polymers simultaneously form (h00) and (0h0) lamellar structures. In particular, (010) peaks involved with π–π stacking are exhibited at 23.63°, 24.42°, 24.12°, and 25.02°, respectively. Based on of a calculation using Bragg's law (i.e., $\lambda = 2d\sin\theta$), π–π stacking distances (d_π) are 3.77, 3.65, 3.69, and 3.56 Å, respectively. The d_π-spacing (i.e., the length between the inter-chains of the PfToBT, PbToBT, PfTDPP, and PbTDPP polymers) decreases when going from using fusedthiophene donor to bithiophene donor and when changing the acceptor unit from oBT to DPP. This is in good agreement with the research published by Ong et al., where bithiophene release space for the side-chain to interpenetrate with the polymers.[45]

Figure 5(b,c) presents the XRD profiles of the polymer:$PC_{70}BM$ blended thin films performed in the out-of-plane and inplane mode, respectively. In the out-of-plane mode, strong (010) diffraction peaks for the polymer:

$PC_{70}BM$ blend films are measured at 18.87°, 18.87°, 18.81°, and 18.81° due to the crystallinity of fullerene. 2θ value of the PfToBT, PbToBT, PfTDPP, and PbTDPP:$PC_{70}BM$ thin films, (010) peaks, observed at 26.77°, 26.89°, 26.71°, and 26.95°, respectively. The calculated interlamellar (d_π) spacings of the blend thin films are 3.33, 3.32, 3.34, and 3.31 Å, respectively. This suggests that the polymer: $PC_{70}BM$ blended films form (0h0) lamellar structure. When a π–π stacking peak is shown for the (010) plane in the out-of-plane mode, it has highly possibility that the thin films adopts a crystalline form with face-on or edge-on orientation. This can be verified by acquiring XRD data using an inplane mode. Figure 5(c) presents the XRD diffraction patterns of the polymer:$PC_{70}BM$ blend thin films detected in the in-plane mode.

The XRD profiles for all of the polymer:PCBM blend films in the in-plane mode show diffraction peaks at high angles. The aforementioned XRD data imply that polymer:$PC_{70}BM$ blend films have edge-on structures in the thin film. In the in-plane mode, the d_π-spacings of the PfToBT, PbToBT, PfTDPP, and PbTDPP: $PC_{70}BM$ thin films are similar with the calculated values in the out-of-plane mode (3.32 3.29, 3.31, and 3.28 Å). For the blended films, the polymers using bithiophene donor also show closer intermolecular distances than the polymers using fusedthiophene donor.

Cross-Sectional SEM and XPS Depth Profile Measurements

In order to examine the composition gradient in the polymer:$PC_{70}BM$ BHJ layer, cross-sectional SEM images were collected and atomic concentration of thiophene (characteristic of polymers and PEDOT:PSS), oxygen (characteristic of polymers side-chain and $PC_{70}BM$), and nitrogen (characteristic of polymers side-chain only) were investigated using XPS depth profile, as shown in Figure 6. The component layers of the device are clearly seen in SEM images. Samples were prepared in simplified structure as ITO glass/PEDOT:PSS/Polymer:$PC_{70}BM$/Al. The thicknesses of the optimum devices measured from SEM images are in good agreement with those measured by α-step (ITO = 170–180 nm, PEDOT:PSS = 30 nm, active layer = 100–110 nm and Al = 150 nm). The depth profile correctly reflects the multilayer structure of the polymer solar cell device. It can be concluded that such a profiling technique is suitable for profiling the cross sectional construction of these devices. We therefore performed XPS profiling of these cross-sections with regards to sulfur (S), oxygen (O), and nitrogen (N) to investigate the vertical distribution of polymer chains and $PC_{70}BM$ within the BHJ films. In XPS images, the BHJ films have a different network between polymer chains and $PC_{70}BM$ from PEDOT:PSS layer (the bottom) to Al electrode layer (the top).

At the top-most surface, all of the polymer:$PC_{70}BM$ blend films show high concentrations of O. This implies that polymer side-chain or $PC_{70}BM$ which contain the O sources are present at the top of the active layer. PbToBT, PfTDPP, and PbTDPP polymer:$PC_{70}BM$ blend films also show high N concentrations at their top-most surfaces. The decrease of N ratio in the active layer region indicates that the N-rich side chains diffuse into the surface of active layer. In particular, this implies that the side chains of the polymers are oriented look upward in the active layer. On the other hand, the PfToBT:$PC_{70}BM$ blend film shows a lower concentration of N at its surface. The N ratio increases in the bottom of the active layer region, indicating that the N-rich side chains diffuse into the bottom of active layer and side-chain of PfToBT are oriented look down. The polymer side chains have both O and N in the same ratio. In the PbToBT, PfTDPP and PbTDPP:$PC_{70}BM$ blend films, the concentration of O is higher than N in the active layer due to the presence of $PC_{70}BM$. In the bottom of the active layer, PfTDPP and PbTDPPs:$PC_{70}BM$ blend films show decreased amounts of O, but the PbToBT:$PC_{70}BM$ blend film has an unchanged amount of O. This indicates that PfTDPP and PbTDPPs:$PC_{70}BM$ blend films have $PC_{70}BM$ that diffuses into the top of active layer, while in the PbToBT:$PC_{70}BM$ blend film that $PC_{70}BM$ diffuses into the bottom of active layer. The PfToBT:$PC_{70}BM$ blend film has a lower concentration of O at the boundary between the HTL and active layer, indicated by the fact that the PfToBT:$PC_{70}BM$ blend film has $PC_{70}BM$ in the top of the layer in the absence of polymer side chains.

As shown in Figure 4, we confirmed that the electron clouds of PfToBT, PbToBT, PfTDPP and PbTDPP are localized on the acceptor oBT and DPP grafted side-chain units. The grafted side chains of PbToBT (or PfToBT) and $PC_{70}BM$ exist on different sides of the active layer and do not come into contact, and as such. These films have difficulty in obtaining efficient charge transfer from polymer to $PC_{70}BM$.

Conversely, PfTDPP (or PbTDPP) and $PC_{70}BM$ exist on the same side of the active layer, and these films have clear intermolecular charge transfer from polymer to $PC_{70}BM$.

Increased concentrations of S and O are indicative of the HTL layer, which consists of PEDOT:PSS. Below the HTL, decreasing S and increasing O are observed in the ITO and glass substrate areas. It is noteworthy that although the total thickness of the organic layer is thinner than thickness of the inorganic layer, the time required to remove the organic layer is longer. The apparent slower sputtering rate of the organic layer can be attributed to ion-induced cross-linkage between organic molecules.[46]

This optimized vertical morphology promotes hole and electron transport along the respective pathways of the polymers and fullerenes in the vertical direction, leading to high Jsc and FF.

Photovoltaic Device Characteristics

BHJ PSCs with ITO/PEDOT:PSS/polymer:$PC_{70}BM$/BaF_2/Ba/Al structures were fabricated to determine the photovoltaic (PV) properties of graft-type polymers. The J–V curves acquired with different $PC_{70}BM$ ratio are shown in Figure 7(a,b). And incident photon to charge carrier efficiency (IPCE) profiles are presented in Figure 7(c). The

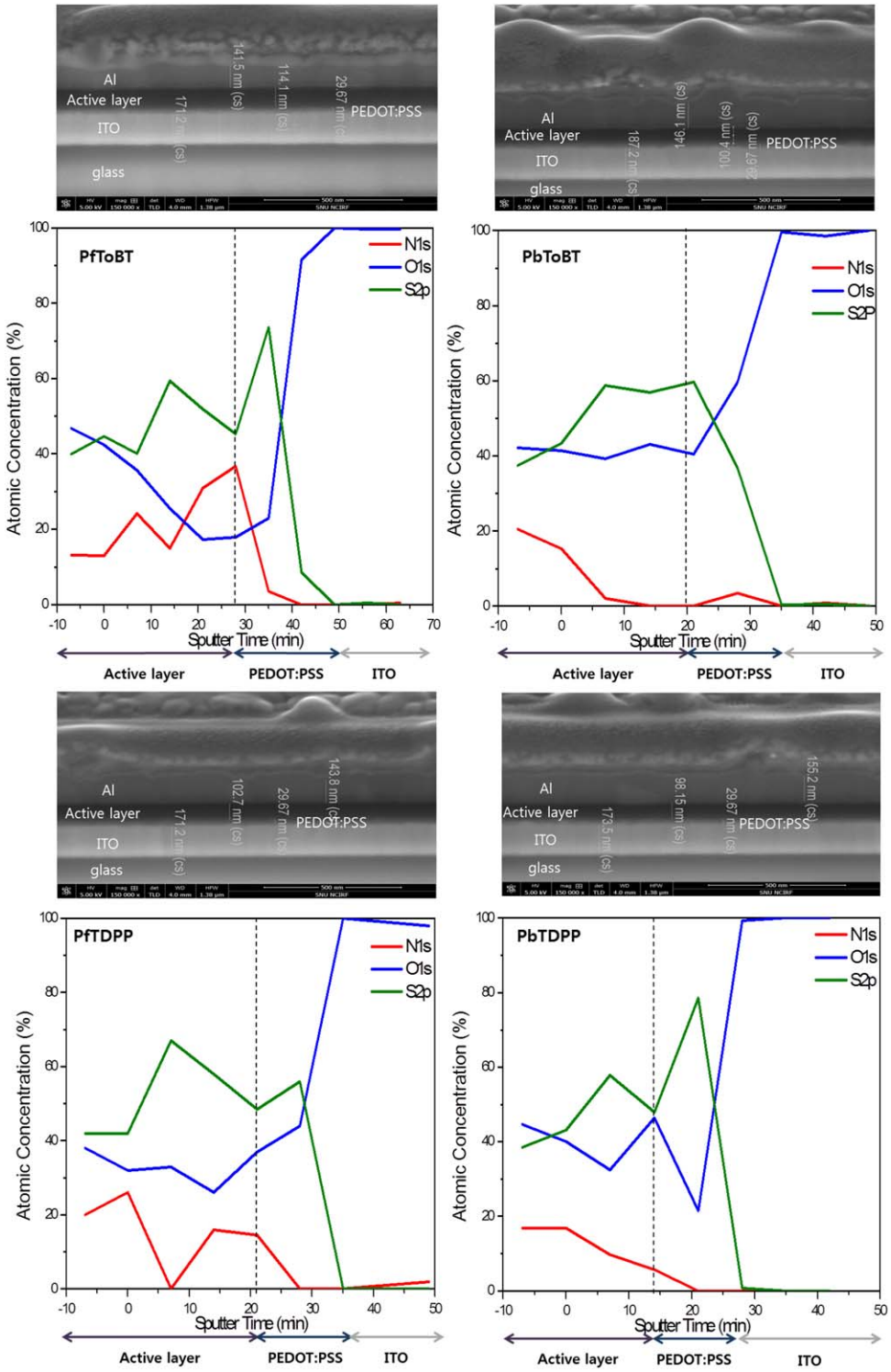

FIGURE 6 Cross-sectional SEM images and XPS depth profile of conventional device with recorded elements of S (resolved to sulfonate and thiophene), O (polymer side-chain and $PC_{70}BM$) and N (polymer side-chain). [Color figure can be viewed in the online issue, which is available at wileyonlinelibrary.com.]

manufactured devices were encapsulated in a glove box. The current density–voltage (J–V) plots were determined under an ambient atmosphere with a 4 mm^2 active area and were estimated under standard AM 1.5G, 100 mW/cm^2 illumination. The polymer:$PC_{70}BM$ weight ratios used in the measurement were 1:2 and 1:3, and the optimized conditions were 1:2 (PfToBT, PbToBT) and 1:3 (PfTDPP, PbTDPP), respectively. σ-dichlorobenzene(ODCB) was used as a solvent

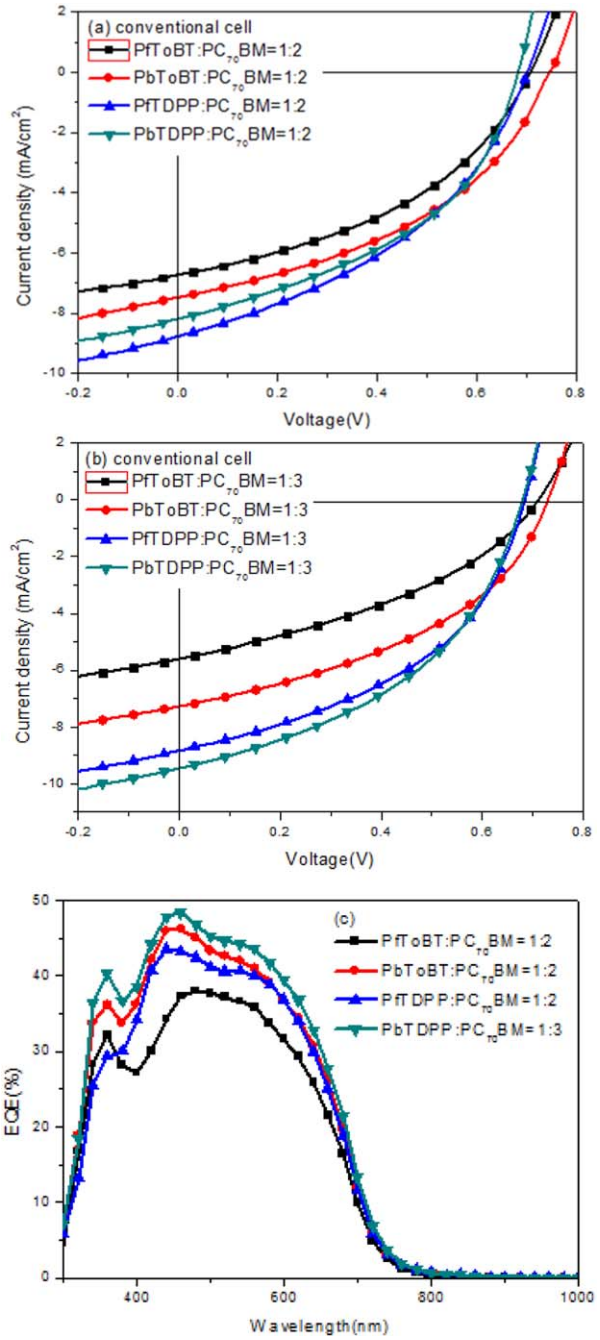

FIGURE 7 The device characteristics of PSC based on polymer: $PC_{70}BM$ with different weight ratio in 1:2 (w/w) (a) and 1:3 (w/w) (b). The IPCE spectra (c). [Color figure can be viewed in the online issue, which is available at wileyonlinelibrary.com.]

to spin-coat the active layers. Table 4 summarizes the photovoltaic response data including V_{OC}, J_{SC}, FF, and PCE.

PfToBT has a PCE of 2.0%, with an open circuit voltage (Voc) of 0.717 V, short-circuit current density (Jsc) of 6.8 $mAcm^2$, and the FF of 41.0%. In PbToBT, a PCE of 2.5% is observed under a Voc of 0.737 V, Jsc of 7.4 mA/cm^2, and FF of 43.1%. PfTDPP exhibits a PCE of 2.7% under a Voc of 0.677 V, Jsc of 8.8 mA/cm^2, and FF of 45.5% and PbTDPP exhibits a PCE of 2.9% under a Voc of 0.677 V, Jsc of 9.4 mA/cm^2, and FF of 44.4%. PCE values were recorded that Jsc of PfToBT and PbToBT is low because of the exciton dissociation rate is low. In particular, the low Jsc are measured for PfToBT and PbToBT because these polymers have difficulty in contacting the polymer side-chain and $PC_{70}BM$ in blend films. When DPP is used as a conjugated side-chain, the bandgap decreases and the extinction coefficient increases because of strong electron affinity. Moreover, the side chains of PfTDPP and PbTDPP easily make contact with $PC_{70}BM$, causing an increase in Jsc and overall device performance. However, V_{OC} is determined according to the gap between the LUMO levels of $PC_{70}BM$ and the HOMO level of the polymer. The oxidation stability decreases when using DPP as the acceptor unit, leading to upshift the HOMO level and reduce the V_{OC} values. The *V*oc of PfTDPP and PbTDPP decrease compared to those of PfToBT and PbToBT.

The shapes of IPCE spectra of the devices are similar to each other. These devices exhibit sufficiently broad IPCE spectra in the visible region (300–800 nm). And higher external quantum efficiency (EQE) values in the UV–vis absorbance range of polymers but lower values above 800 nm. The PbTDPP:$PC_{70}BM$ blend-used cell showed the highest EQE that is agree with the highest photo current, in which the values reached 48.41% at ~460 nm. PfToBT, PbToBT, and PfTDPP recorded 38.04, 43.61, and 46.16%, respectively.

Hole Carrier Mobility and Morphological Properties

In BHJ solar cells, Jsc and FF are directly limited by the hole mobility of the polymer, making it a crucial parameter for determining photovoltaic performance. We determined the hole mobility of the polymer and $PC_{70}BM$ blend films from the logJ versus logV graphs presented in the Supporting Information, Figures S12–S15 and Table S1 via a space charge limited current (SCLC) method. A structure of hole-only devices in this work is ITO/PEDOT:PSS/Polymer:$PC_{70}BM$/MoO_3/Al.

Based on the equation and the logJ versus logV graph, the hole mobility values of PfToBT, PbToBT, PfTDPP, and PbTDPP blended with $PC_{70}BM$ are 3.85×10^{-4}, 2.13×10^{-3}, 2.52×10^{-3}, and 2.66×10^{-3} [$cm^2/(V\ s)$], respectively. The

TABLE 4 Device Performances of Polymers with Different $PC_{70}BM$ Ratio

Polymer	$PC_{70}BM$ Ratios	Jsc (mA/cm^2)	Voc (V)	FF (%)	PCE (%)
PfToBT	1:2	6.8	0.717	41.0	2.0
	1:3	5.6	0.717	37.6	1.6
PbToBT	1:2	7.4	0.737	43.1	2.5
	1;3	7.2	0.737	42.1	2.2
PfTDPP	1:2	8.7	0.697	41.1	2.5
	1:3	8.8	0.677	45.5	2.7
PbTDPP	1:2	8.1	0.677	44.6	2.5
	1:3	9.4	0.677	44.4	2.9

conformation of the polymer film, which influences the charge-transfer pathway, affected to the hole mobility of the polymers. PfToBT and PbToBT with difficult charge dissociation have a poor hole mobility, leading to low J_{SC} values in their fabricated photovoltaic cells.

The active layer surface morphology is a very critical parameter for determining the efficiency of PSCs. So, the morphologies of the active layers were identified via AFM and presented in Supporting Information Figure S16. The light-colored and dark-colored areas correspond to polymers and PCBM domains, respectively. The polymer:$PC_{70}BM$ blended films have a smooth surface due to its nanoscale features and had a low root-mean-square(RMS) roughness of 0.63–0.75 nm. These were shown excellent intermixing between the polymer and $PC_{70}BM$ which enhanced development of pathway by the polymers.

CONCLUSION

In this study, four graft-type polymers prepared with different types of donor and acceptor, PfToBT, PbToBT, PfTDPP, and PbTDPP, were successfully synthesized via the Stille coupling reaction. PfTDPP and PbTDPP exhibit broader absorption region and high absorption coefficients because of the strong electron affinity of the DPP group. All the polymers:$PC_{70}BM$ blend films had edge-on structure, and the d_{π}-spacings of the polymer:$PC_{70}BM$ thin films have similar values of 3.33, 3.32, 3.34, and 3.31 Å, respectively. However, the distribution rate of polymer and $PC_{70}BM$ was different throughout the active layer. The grafted side-chain of PfToBT and PbToBT:$PC_{70}BM$ existed on different sides of the active layer, and conjugated side chains with localized electron clouds did not come into contact with $PC_{70}BM$ due to charge dissociation and electron transfer. On the other hand, the PfTDPP and PbTDPP:$PC_{70}BM$ blend films indicated that $PC_{70}BM$ coexisted in the top of the layer with the conjugated side chains of the polymer. These had efficient charge transfer from polymer to $PC_{70}BM$ and showed higher Jsc. PbTDPP showed values of 9.4 mA/cm^2, 0.677 V, 44.4, and 2.9%, respectively, demonstrating the best performance.

ACKNOWLEDGMENTS

This research was supported by the New and Renewable Energy Core Technology Program of the Korea Institute of Energy Technology Evaluation and Planning (KETEP) grant funded by the Ministry of Trade, Industry and Energy (MI, Korea) (No. 20133030000180) and New and Renewable Energy Core Technology Program of the Korea Institute of Energy Technology Evaluation and Planning (KETEP), grant financial resource from the Ministry of Trade, Industry and Energy, Republic of Korea (No. 20153010140030).

REFERENCES AND NOTES

1 F. C. Krebs, N. Espinosa, M. Hösel, R. R. Søndergaard, M. Jørgensen, *Adv. Mater.* **2014**, *26*, 29–39.

2 L. Lu, T. Zheng, Q. Wu, A. M. Schneider, D. Zhao, L. Yu, *Chem. Rev.* **2015**, *115*, 12666–12731.

3 K. H. Kim, H. Kang, H. J. Kim, P. S. Kim, S. C. Yoon, B. J. Kim, *Chem. Mater.* **2012**, *24*, 2373–2381.

4 M. A. Green, K. Emery, Y. Hishikawa, W. Warta, E. D. Dunlop, *Prog. Photovolt. Res. Appl.* **2016**, *24*, 3–11.

5 M. H. Choi, K. W. Song, D. K. Moon, *Polym. Chem.* **2015**, *6*, 2636–2646.

6 M. L. Keshtov, S. A. Kuklin, F. C. Chen, A. R. Khokhlov, R. Kurchania, G. D. Sharma, *J. Polym. Sci. A: Polym. Chem.* **2015**, *53*, 2390–2398.

7 Z. G. Zhang, Y. Li, *Sci. China Chem.* **2014**, *58*, 192–209.

8 Y. Huang, X. Guo, F. Liu, L. Huo, Y. Chen, T. P. Russell, C. C. Han, Y. Li, J. Hou, *Adv. Mater.* **2012**, *24*, 3383–3389.

9 S. H. Liao, H. J. Jhuo, Y. S. Cheng, S. A. Chen, *Adv. Mater.* **2013**, *25*, 4766–4771.

10 S. H. Liao, H. J. Jhuo, P. N. Yeh, Y. S. Cheng, Y. L. Li, Y. H. Lee, S. Sharma, S. A. Chen, *Sci. Rep.* **2014**, *4*, 6813.

11 C. Wang, B. Zhao, Z. Cao, P. Shen, Z. Tan, X. Li, S. Tan, *Chem. Commun.* **2013**, *49*, 3857–3859.

12 Y. Li, *Acc. Chem. Res.* **2012**, *45*, 723–733.

13 P. Shen, H. Bin, L. Xiao, Y. Li, *Macromolecules* **2013**, *46*, 9575–9586.

14 Y. R. Liu, L. H. Chan, H. Y. Tang, *J. Polym. Sci. A: Polym. Chem.* **2015**, *53*, 2878–2889.

15 J. Hou, Z. a. Tan, Y. Yan, Y. He, C. Yang, Y. Li, *J. Am. Chem. Soc.* **2006**, *128*, 4911–4916.

16 Z. Gu, P. Tang, B. Zhao, H. Luo, X. Guo, H. Chen, G. Yu, X. Liu, P. Shen, S. Tan, *Macromolecules* **2012**, *45*, 2359–2366.

17 Z. Gu, P. Shen, S. W. Tsang, Y. Tao, B. Zhao, P. Tang, Y. Nie, Y. Fang, S. Tan, *Chem. Commun.* **2011**, *47*, 9381–9383.

18 H. Padhy, J. H. Huang, D. Sahu, D. Patra, D. Kekuda, C. W. Chu, H. C. Lin, , *J. Polym. Sci. A: Polym. Chem.* **2010**, *48*, 4823–4834.

19 V. Tamilavan, K. H. Roh, R. Agneeswari, D. Y. Lee, S. Cho, Y. Jin, S. H. Park, M. H. Hyun, *J. Polym. Sci. A: Polym. Chem.* **2014**, *52*, 3564–3574.

20 D. Cortizo-Lacalle, S. Arumugam, S. E. T. Elmasly, A. L. Kanibolotsky, N. J. Findlay, A. R. Inigo, P. J. Skabara, *J. Mater. Chem.* **2012**, *22*, 11310–11315.

21 H. Bronstein, Z. Chen, R. S. Ashraf, W. Zhang, J. Du, J. R. Durrant, P. Shakya Tuladhar, K. Song, S. E. Watkins, Y. Geerts, M. M. Wienk, R. A. J. Janssen, T. Anthopoulos, H. Sirringhaus, M. Heeney, I. McCulloch, *J. Am. Chem. Soc.* **2011**, *133*, 3272–3275.

22 C. H. Woo, P. M. Beaujuge, T. W. Holcombe, O. P. Lee, J. M. J. Fréchet, *J. Am. Chem. Soc.* **2010**, *132*, 15547–15549.

23 J. C. Bijleveld, V. S. Gevaerts, D. Di Nuzzo, M. Turbiez, S. G. J. Mathijssen, D. M. de Leeuw, M. M. Wienk, R. A. J. Janssen, *Adv. Mater.* **2010**, *22*, E242–E246.

24 P. Sonar, S. P. Singh, E. L. Williams, Y. Li, M. S. Soh, A. Dodabalapur, *J. Mater. Chem.* **2012**, *22*, 4425–4435.

25 Y. Sun, S. C. Chien, H. L. Yip, K. S. Chen, Y. Zhang, J. A. Davies, F. C. Chen, B. Lin, A. K. Y. Jen, *J. Mater. Chem.* **2012**, *22*, 5587–5595.

26 K. W. Song, M. H. Choi, H. J. Song, S. W. Heo, J. Y. Lee, D. K. Moon, *Solar Energy Mater. Solar Cells* **2014**, *120,* 303–309.

27 M. Helgesen, S. A. Gevorgyan, F. C. Krebs, R. A. J. Janssen, *Chem. Mater.* **2009**, *21*, 4669–4675.

28 L. Huo, J. Hou, H. Y. Chen, S. Zhang, Y. Jiang, T. L. Chen, Y. Yang, *Macromolecules* **2009**, *42*, 6564–6571.

29 J. Hou, L. Huo, C. He, C. Yang, Y. Li, *Macromolecules* **2006**, *39*, 594–603.

30 X. Liu, Y. Huang, Z. Cao, C. Weng, H. Chen, S. Tan, *Polym. Chem.* **2013**, *4*, 4737–4745.

31 C. Y. Kuo, Y. C. Huang, C. Y. Hsiow, Y. W. Yang, C. I. Huang, S. P. Rwei, H. L. Wang, L. Wang, *Macromolecules* **2013**, *46*, 5985–5997.

32 M. H. Choi, K. W. Song, S. W. Heo, Y. W. Han, D. K. Moon, *J. Indus. Eng. Chem.* **2015**, *26*, 173–181.

33 J. C. Bijleveld, A. P. Zoombelt, S. G. J. Mathijssen, M. M. Wienk, M. Turbiez, D. M. de Leeuw, R. A. J. Janssen, *J. Am. Chem. Soc.* **2009**, *131*, 16616–16617.

34 Z. Chen, M. J. Lee, R. Shahid Ashraf, Y. Gu, S. Albert-Seifried, M. Meedom Nielsen, B. Schroeder, T. D. Anthopoulos, M. Heeney, I. McCulloch, H. Sirringhaus, *Adv. Mater.* **2012**, *24*, 647–652.

35 M. M. Wienk, M. Turbiez, J. Gilot, R. A. J. Janssen, *Adv. Mater.* **2008**, *20*, 2556–2560.

36 H. Li, H. Luo, Z. Cao, Z. Gu, P. Shen, B. Zhao, H. Chen, G. Yu, S. Tan, *J. Mater. Chem.* **2012**, *22*, 22913–22921.

37 P. Leriche, P. Frère, A. Cravino, O. Alévêque, J. Roncali, *J. Org. Chem.* **2007**, *72*, 8332–8336.

38 J. K. Jin, J. K. Choi, B. J. Kim, H. B. Kang, S. C. Yoon, H. You, H. T. Jung, *Macromolecules* **2011**, *44*, 502–511.

39 S. C. Price, A. C. Stuart, W. You, *Macromolecules* **2010**, *43*, 4609–4612.

40 H. Tan, X. Deng, J. Yu, B. Zhao, Y. Wang, Y. Liu, W. Zhu, H. Wu, Y. Cao, *Macromolecules* **2013**, *46*, 113–118.

41 H. Zhou, L. Yang, S. Xiao, S. Liu, W. You, *Macromolecules* **2009**, *43*, 811–820.

42 Q. Zheng, B. J. Jung, J. Sun, H. E. Katz, *J. Am. Chem. Soc.* **2010**, *132*, 5394–5404.

43 J. L. Brédas, D. Beljonne, V. Coropceanu, J. Cornil, *Chem. Rev.* **2004**, *104*, 4971–5004.

44 Z. Ma, E. Wang, M. E. Jarvid, P. Henriksson, O. Inganas, F. Zhang, M. R. Andersson. *J. Mater. Chem.* **2012**, *22*, 2306–2314.

45 B. S. Ong, Y. Wu, P. Liu, S. Gardner, *J. Am. Chem. Soc.* **2004**, *126*, 3378–3379.

46 H. Choi, S. J. Ko, T. Kim, P. O. Morin, B. Walker, B. H. Lee, M. Leclerc, J. Y. Kim, A. J. Heeger, *Adv. Mater.* **2015**, *27*, 3318–3324.